Two-Step Phase Separation in Polymer Blends

Ian C. Henderson and Nigel Clarke*

Department of Chemistry, University Science Laboratories, South Road, Durham DH1 3LE, United Kingdom

Received May 29, 2003; Revised Manuscript Received January 13, 2004

ABSTRACT: A two-step quench process is modeled using Cahn−Hilliard theory for symmetric binary polymer mixtures. The blend is quenched from a stable state in the one-phase region to an unstable state in the two-phase region where it undergoes spinodal decomposition. The mixture is allowed to coarsen for two different time periods before a second quench was applied to a point further inside the unstable region. During the initial stages following the second quench smaller secondary domains appeared briefly in the primary domains obtained from the first quench step. The peak arising from the second quench step was isolated from the structure factor, and the early growth stages were investigated using linearized theory. We also quantify the maximum degree of secondary phase separation as a function of quench depth, which we hope will provide stimulus for further experimental studies.

Introduction

Phase separation in polymer blends is of interest from both fundamental and applied points of view. Numerous studies, both theoretical and experimental, have been reported on the dynamics of phase separation in polymer solutions and blends following a temperature jump or quench from the one-phase region of the phase diagram. The time evolution of phase-separating domain structures via spinodal decomposition (SD) when the mixed blend becomes unstable rather than metastable is of particular interest. A theory for the process was first proposed by Cahn and Hilliard[1] for binary metal alloys. This was extended to polymeric systems by de Gennes,[2] Pincus,[3] and Binder[4] by combination with the well-known Flory−Huggins[5] theory.

Phase separation occurs when a polymer blend is quenched from the one-phase region into the two-phase unstable region. Here concentration fluctuations become unstable and grow, rather than decay, giving domains rich in one polymeric species. The Cahn−Hilliard theory can be solved analytically to predict the characteristics of the early stages of growth and numerically to study the later stages of growth. It has been shown that initially fluctuations above a critical wavelength grow exponentially with a particular length scale dominating. Eventually coarsening of the domains occurs to reduce the interfacial area.[6−10] During the late stages, the characteristic length scale scales with time as $t^{1/3}$. Pioneering analytical studies of the intermediate and late stages have also been carried out by Langer[11] and Akcasu and Klein.[12]

The theory has been extended to consider more complex mixtures. For example, the original model assumes the two components are monodisperse; however, polymers are often rather polydisperse. Hence, analytical theories of the early stages of phase separation for polydisperse polymers have been proposed,[13−16] and numerical studies of the intermediate and later stages have also been undertaken.[17] Surprisingly, it has been shown that polydispersity has little effect on the details of the phase separation process. The wide applicability of the theory has also been utilized to study, for example, solid nanoparticles dispersed in a polymer blend[18,19] to attempt to tailor the morphology and control the macroscopic properties of a composite. The theory has also been extended to "viscoelastic phase separation",[20] in which unusual morphologies develop due to an imbalance in the rheological properties of the two components.

There have been many experimental reports of phase separation in a mixture of polymeric species quenched from the single phase to a temperature inside the spinodal region. More recently, two-step temperature jumps have been studied experimentally[21−24] using light scattering techniques. Hayashi et al.[22,24] studied the time evolution of the structure factor and the early stages of the second step, which they found to be well characterized by linearized theory. The same group found that after the second temperature jump the structure grew according to the scaling laws that are relevant to a single-step SD experiment.[23] Theoretical studies in this area are limited; Fialkowski and Holyst[25] have recently studied relaxation of structures during quenches into the two-phase region followed by a jump back into the single-phase region, and Clarke[26] has investigated target morphologies using a method similar to the two-step process used here.

In this paper, a two-step process is studied theoretically. A polymeric mixture is quenched from the single phase at T_0 to a phase-separated structure at T_1. Then after some domain growth has occurred another quench to T_2 further within the phase-separated regime is carried out. The linearized theory of Cahn[27] has previously been used to assess the early stage growth of a single quench system and will be used here to probe the early growth stages of the secondary quench. We also consider the effect that quench depth has on the degree of secondary phase separation that occurs.

Model and Numerical Procedure

For simplicity, a symmetric binary system is considered, in which both components have the same degree of polymerization, N. Hydrodynamic effects are neglected as although they play an important role in the late stages of phase separation during coarsening, the development of the early stages should not be affected,

* Corresponding author. E-mail Nigel.Clarke@durham.ac.uk.

10.1021/ma034718l CCC: $27.50
Published on Web 02/13/2004

and we are interested in the structure development immediately after the second quench. The starting point for the model is a continuity equation for each component present. The continuity equation expresses the conservation of mass in the system and relates the time and spatial dependencies of the concentration of a species i, $\phi_i(r,t)$, to the mass current, $j_i(r,t)$. The mass current is related thermodynamically to the free energy functional through the chemical potential and Cook[28] modified the Cahn−Hilliard model to include noise. This resultant Cahn−Hilliard−Cook nonlinear diffusion equation may be written

$$\frac{\partial\phi}{\partial t} = \nabla\cdot D\nabla\frac{\delta F\{\phi(\mathbf{r},t)\}}{\delta\phi(\mathbf{r},t)} + \eta(\mathbf{r},t) \tag{1}$$

where D is the self-diffusion coefficient which we shall assume to be constant, $\phi(r,t)$ is the volume fraction of component A, and η is the thermal noise. The model is extended to polymer blends by using Flory−Huggins theory to determine the free energy of mixing per lattice site for an incompressible, two-component polymer blend

$$\frac{f_{FH}(\phi)}{k_B T} = \frac{\phi}{N_A}\ln\phi + \frac{1-\phi}{N_B}\ln(1-\phi) + \chi\phi(1-\phi) \tag{2}$$

where N_A (N_B) is the degree of polymerization of the polymeric species A (B), χ is the Flory interaction parameter, and $\phi_B(r,t) = 1 - \phi(r,t)$ is the volume fraction of component B, such that the blend is incompressible. From the above free energy, for a symmetric blend, i.e., $N_A = N_B = N$, the spinodal curve, given by $\chi_s = 1/[2N\phi(1-\phi)]$, is the boundary between the metastable and the unstable region of phase separation. The binodal curve

$$\chi_B = -\frac{\ln[\phi/(1-\phi)]}{N(1-2\phi)} \tag{3}$$

represents the boundary between metastability and the one-phase region and for a binary monodisperse blend also determines the equilibrium composition of coexisting phases.

De Gennes[2] argued that that chain connectivity manifests itself as an explicit entropic contribution and proposed that in the presence of fluctuations the Flory−Huggins type free energy functional needs to be supplemented with a square gradient term, the coefficient of which is given by the sum of enthalpic and entropic terms:

$$\kappa(\phi) = \frac{1}{36}\left[\frac{{l_A}^2}{\phi(\mathbf{r})} + \frac{{l_B}^2}{1-\phi(\mathbf{r})}\right] + \chi\lambda^2 \tag{4}$$

where l_A (l_B) is the Kuhn length of species A (B) and λ is the interaction distance between monomers. The Flory−Huggins−de Gennes free energy for an incompressible blend therefore becomes

$$\frac{F_{FHdG}\{\phi(\mathbf{r})\}}{k_B T} = \int d\mathbf{r}\left[\frac{f_{FH}[\phi(\mathbf{r})]}{k_B T} + \kappa[\phi(\mathbf{r})]\left|\nabla\phi(\mathbf{r})\right|^2\right] \tag{5}$$

where the integral is performed over the volume of the sample. Preliminary studies showed that the composition-independent term in eq 4 has a negligible effect on structure development, and hence all calculations presented in this paper are performed with $\lambda = 0$. By combining eqs 1 and 4 and by rescaling into a dimensionless form, we arrive at the equation

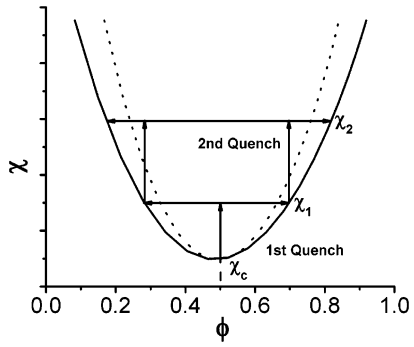

Figure 1. Phase diagram illustrating the two-step quench phase separation process in a symmetric binary polymer blend.

$$\frac{\partial\phi(\mathbf{x},\tau)}{\partial\tau} = \frac{1}{2}\nabla^2\left[\frac{\chi_c}{2(\chi_f-\chi_s)}\ln\frac{\phi}{1-\phi} - \frac{2\chi}{\chi_f-\chi_s}\phi + \frac{1-2\phi}{36\phi^2(1-\phi)^2}(\nabla\phi)^2 - \frac{1}{18\phi(1-\phi)}\nabla^2\phi\right] \tag{6}$$

where χ_c is the value of χ on the spinodal curve at the critical point and χ_f is the deepest quench depth used during the simulation. In the case of the first step, $\chi = \chi_1 = \chi_f$ and $\chi_s = \chi_c$, and in the case of the second step $\chi = \chi_2 = \chi_f$ and χ_s is the spinodal value of χ at $\phi = \phi_0^{(2)}$; i.e., $\chi_s = 1/[2N\phi_0^{(2)}(1-\phi_0^{(2)}]$. In eq 6, $\mathbf{x}$ and τ are the rescaled spatial and temporal variables, respectively, given by $\mathbf{x} = (|\chi_f - \chi_s|)^{1/2}\mathbf{r}/l$ and $\tau = ND(\chi_f - \chi_s)^2 t/l^2$, and the noise term has been neglected.

The evolution during phase separation can be conveniently quantified by the time-dependent structure factor

$$S(\mathbf{k},\tau) = \left\langle\frac{1}{L^d}\sum_{\mathbf{x}}\sum_{\mathbf{x}'} e^{i\mathbf{k}\cdot\mathbf{x}}[\phi(\mathbf{x}+\mathbf{x}',\tau)\,\phi(\mathbf{x}',\tau) - \langle\phi\rangle^2]\right\rangle \tag{7}$$

where L^d is the total number of lattice sites. The wave vectors are defined as $k = (2\pi/L\Delta x)n$, where $n = 1, 2, \ldots, L/2$ and $\langle\ldots\rangle$ denotes an averaging over all possible configurations.

As already noted, eq 6 has been used extensively to study phase separation in polymer mixtures. In this paper we use the model to simulate a two-step quench process. During the simulation an initial quench is carried out from the homogeneous state into the two-phase region of the phase diagram, and the mixture is allowed to evolve to the later stages of SD. In other words, the phase-separated domains first evolve toward the equilibrium composition values as determined by the coexistence curve and then coarsen. Once the late stages of SD have been reached and domain growth has been observed, a second quench is carried out to deeper within the two-phase region. The process is shown schematically in Figure 1.

The first quench was undertaken to $\chi_1 = 0.0104$, with structural evolution being allowed until two different quench times, $\tau_1 = 2500$ and 7500. In each case a well-defined initial structure develops, and then a second quench was applied to three different χ_2 values of 0.0133, 0.0125, and 0.0119. To determine structure factors, each result was averaged over 10 runs, and the

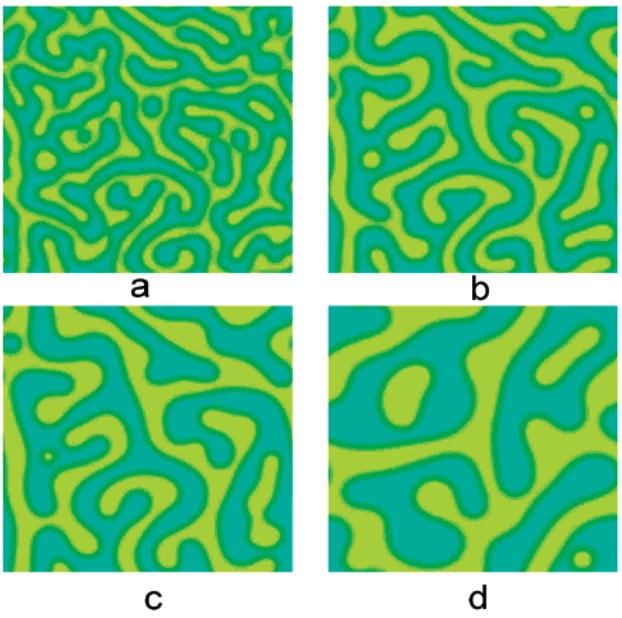

Figure 2. Development of the morphology following a quench into the two-phase region with $\chi_1 = 0.0104$. Quench times after the quench are $\tau_1 =$ (a) 625, (b) 1250, (c) 2500, and (d) 7500. The initial conditions (random noise) were different for (c) and (d); hence, the structure in (d) is not simply a coarsened version of the structure in (c).

only case studied was the symmetric case ($N_A = N_B$). These values of the interaction parameters were chosen to allow us to explore a similar region of the phase diagram studied by Hashimoto et al.[23] While the values of their interaction parameters ($\chi_s = 0.001\,45$, $\chi_1 = 0.001\,51$, and $\chi_2 = 0.001\,75$) differ from our values, our parameters were chosen for computational convenience and to achieve similar values of the equilibrium coexistence compositions after the first and second quench depths. The work was carried out on a 256^2 two-dimensional lattice using periodic boundary conditions; the initial concentration of the matrix was set as $\phi = 0.5$ ($\phi_B = 0.5$) with an initial random noise of ± 0.01 applied at the start of each quench. The Δt (time step) value used during the temporal discretization was 0.0025, and the spatial discretization was $\Delta x = 0.5$. To keep the length scaling of the system consistent, χ_f was fixed throughout the simulation, such that $\chi_f = \chi_2$. This choice of scaling ensures that the lattice size is fine enough to capture the relevant phase separation length scales during both the first and second quenches. The degree of polymerization was chosen such that $\chi_c = 0.01$ for all simulations during both the primary and secondary quenches.

Results

In Figure 2a−c a series of snapshots can be seen which show the growth and broadening of two domains from the single-phase polymeric mixture into a two-phase system. Because of symmetry, the structures exhibit the characteristic co-continuous morphology.

The quench depth corresponds to an equilibrium morphology with $\phi = 0.33$ in the B-rich phases and, due to symmetry, $\phi = 0.67$ in the A-rich phases. Figure 2c,d shows a comparison of the typical morphologies for the two different times at which the second quench was applied. The equilibrium composition within each phase has been reached by $\tau_1 = 625$.

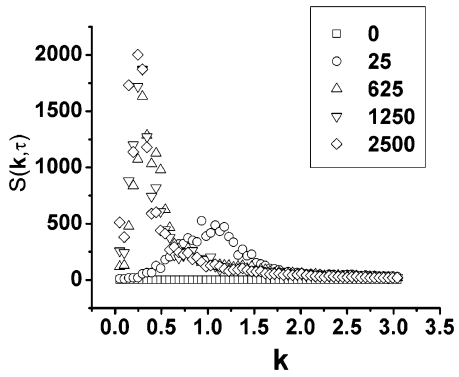

Figure 3. Radially averaged structure factor, $S(\mathbf{k},\tau)$, vs $\mathbf{k}$ for several values of τ_1 and $\chi_1 = 0.0104$.

As already noted, the growth process can be quantified by determining the evolution of the structure factor with quench time, as shown in Figure 3, in which $\mathbf{k}$ is a dimensionless variable, corresponding to the experimental quantity, $q = \mathbf{k}(\chi_f - \chi_s)^{1/2}/l$.

At $\tau_1 = 0$ there is negligible structure since the system is still homogeneous, but as the morphology develops and broadens with quench time, the structure factor increases in intensity with a particular wave vector dominating ($\mathbf{k}_{max}$), and as expected, the position of $\mathbf{k}_{max}$ decreases with quench time. The results thus far have previously been considered in detail by a number of authors;[29] hence, we will not discuss the single quench case further.

The second step was carried out to three different quench depths, $\chi_2 = 0.0133$, 0.0125, and 0.0119, and was again averaged over 10 runs in order to determine the structure factor. An example of the domain growth can be seen in Figure 4.

Note that although experimentally the mobility is temperature and hence quench depth dependent, it is not necessary to explicitly account for this since the time steps are scaled by the mobility. Hence, the difference between mobility during the first and second quench can be reflected in a different scaling factor from numerical time to real time for each of the two stages. Importantly, the structural growth is not affected by this assumption.

As the simulation proceeds, small secondary domains of each polymer appear in the larger primary domains. This is a consequence of the initially favored length scale (the fastest growing fluctuation), as determined from linearized theory, being smaller than the primary structural scale. Although these secondary domains are initially dynamically favorable, they "dissolve" into the surrounding phases since they create large interfacial areas and a large increase in free energy. The structure in Figure 4c is particularly noteworthy: not only are the secondary domains strongly phase separated, the droplets are apparently regularly spaced (as revealed quantitatively by the scattering maximum from the interference of the scattering from secondary domains). This highlights the possibility of using such quench sequences to develop regular morphologies that may have unusual physical properties. Eventually, the original morphology is returned but with concentrations of $\phi = 0.1$ and $\phi_B = 0.9$. This is clearly seen by comparing parts a and f of Figure 4; the structures are very similar, but the contrast between phases has increased. The point at which the second quench step is started to the point at which the original morphology (i.e., no secondary structures) is returned depends on quench depth.

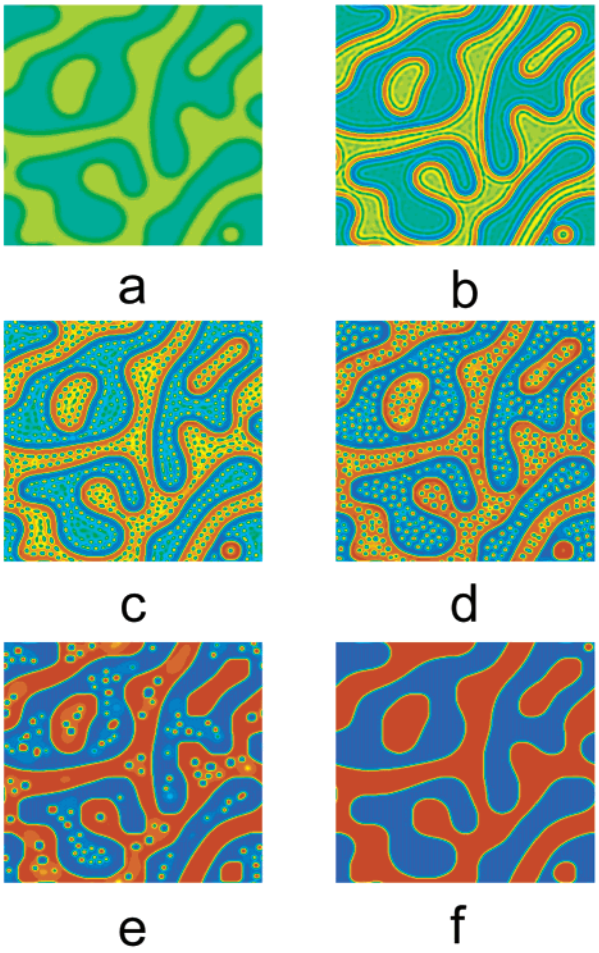

Figure 4. Development of the polymer morphology following a second quench into the two-phase region with $\chi_2 = 0.0133$ and $\tau_1 = 7500$. Quench times after the second quench correspond to $\tau_2 =$ (a) 0, (b) 3.75, (c) 6.25, (d) 12.5, (e) 50, and (f) 375. Extra colors have been added in to improve picture contrast.

The deeper the depth of the quench, the longer it takes to return the morphology to its original state. If the primary morphology is broader, then more time is needed to return to this original morphology.

Figure 5a shows the structure factor at the start of the second quench and after $\tau_2 = 12.5$. The development of the secondary structure manifests itself as a weak but distinct shoulder. From eq 6 growth of the form

$$S(\mathbf{k},\tau_2)/S(\mathbf{k},\tau_2 = 0) = \exp\{R(\mathbf{k})\tau_2\} \qquad (8)$$

where $R(\mathbf{k})$ is the growth rate of fluctuations with wavevector $\mathbf{k}$, is predicted for a quench from a homogeneous state with only very weak fluctuations. However, the presence of the secondary structure is a consequence of the behavior of such fluctuations superimposed on a inhomogeneous background; hence, it seems reasonable to factor out the structure factor at the start of the second quench. Figure 5b−g shows the growth of this secondary peak.

As τ_2 increases, the magnitude of the secondary peak also increases. Eventually the peak stops increasing in magnitude and decays as the secondary structure disappears, as can be seen in Figure 6.

During the early stages of growth it was found that the structure factor initially increased exponentially with time as shown in Figure 7.

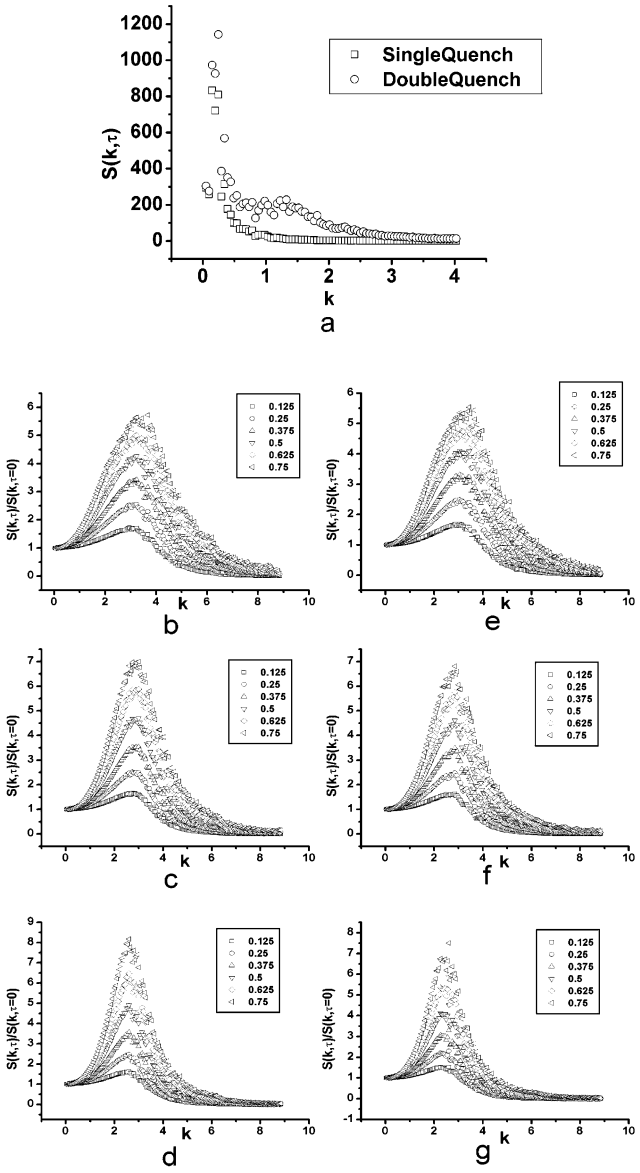

Figure 5. Development of the structure factor: (a) a comparison of $S(\mathbf{k})$ immediately prior to the second quench at $\tau_2 = 12.5$, for $\chi_2 = 0.0133$ and $\tau_1 = 7500$, (b−g) for various values of τ_2 as shown in the legend, after a primary quench of $\tau_1 = 2500$ for (b) $\chi_2 = 0.0119$, (c) $\chi_2 = 0.0125$, (d) $\chi_2 = 0.0133$, and $\tau_1 = 7500$ for (e) $\chi_2 = 0.0119$, (f) $\chi_2 = 0.0125$, and (g) $\chi_2 = 0.0133$. In (b−g), $S(\mathbf{k})$ at each time step has been divided by the values of $S(\mathbf{k})$ when the second quench was initiated.

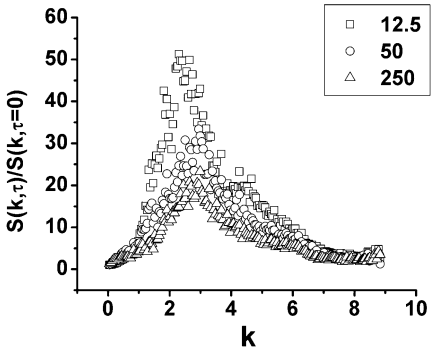

Figure 6. Decrease in magnitude of secondary structure factor for three values of τ_2, with $\chi_2 = 0.0133$ and $\tau_1 = 7500$.

Note that we also considered the effect of subtracting the $S(\mathbf{k}, \tau_2 = 0)$; however, this resulted in less well-

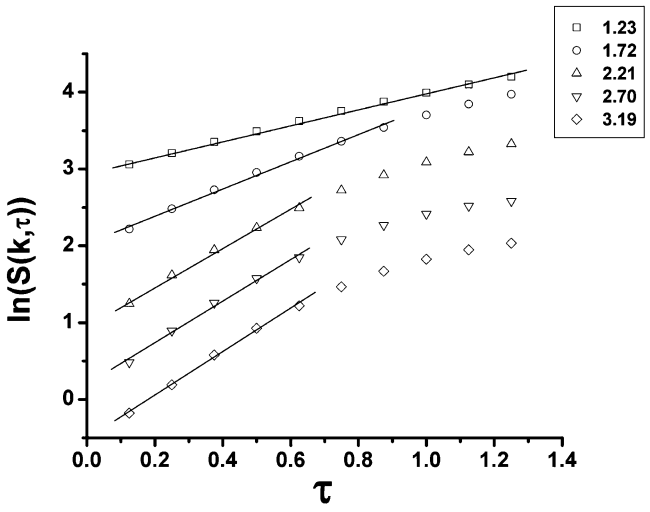

Figure 7. Growth of the structure factor, $S(\mathbf{k},\tau)$, with time, τ_2, for various wavevectors, $\mathbf{k}$, as indicated in the legend, after $\tau_1 = 2500$ and with $\chi_2 = 0.0119$. The lines show the fitting used to determine the growth rates during the early stages.

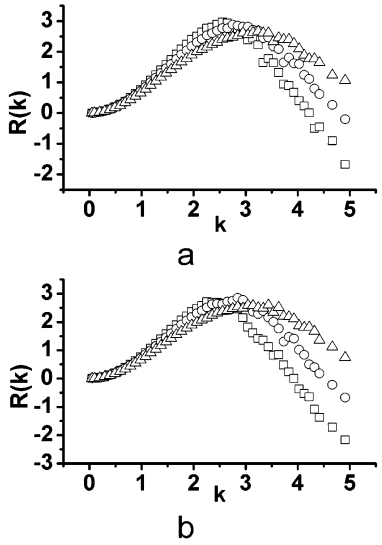

Figure 8. Early stage growth and decay of secondary structure analyzed using linearized theory for (a) $\tau_1 = 2500$ and (b) $\tau_1 = 7500$ and three quench depths of $\chi_2 = 0.0119$ (□), 0.0125 (○), and 0.0133 (Δ).

defined secondary structure factors that did not show exponential growth. The factorization may not however necessarily be legitimate in the later stages of the second step phase separation in which nonlinear effects in the time evolution process become increasingly important.

By fitting the numerical results to eq 8, we have determined the growth rates $R(\mathbf{k})$, as shown in Figure 8.

From linearization of eq 6, assuming a homogeneous initial mixture, the growth rate during the early stages can be written as

$$R(\mathbf{k}) = -\frac{1}{2}\left[\frac{1}{N(\chi_f - \chi_s)\phi_0(1-\phi_0)} - \frac{2\chi}{\chi_f - \chi_s}\right]\mathbf{k}^2 - \frac{1}{36\phi_0(1-\phi_0)}\mathbf{k}^4 \quad (9)$$

so that, with the scaling used in our model, the fastest growing wave vector corresponds to

Table 1. Comparison of the Predicted and Observed Fastest Growing Wavevectors as a Function of Secondary Quench Depth

	$\mathbf{k}_{max}$		
χ	predicted	$\tau_1 = 2500$	$\tau_1 = 7500$
0.0119	1.1	3.2	3.4
0.0125	1.6	2.8	2.8
0.0133	2.1	2.5	2.3

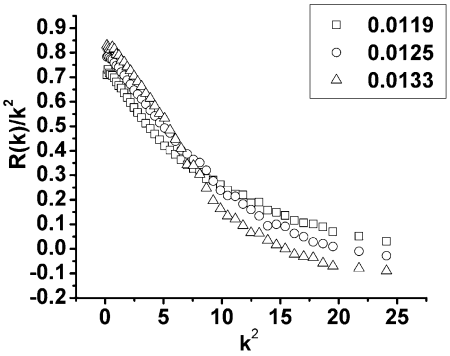

Figure 9. Plot of $R(\mathbf{k})/\mathbf{k}^2$ vs $\mathbf{k}$, showing that linearity is observed only for smaller values of $\mathbf{k}$.

$$\mathbf{k}_{max}{}^2 = -\frac{18}{\chi_f - \chi_s}[\chi_f\phi_0^{(2)}(1-\phi_0^{(2)}) - \chi_s\phi_0^{(1)}(1-\phi_0^{(1)})] \quad (10)$$

where $\phi_0^{(1)}$ is the volume fraction ($\phi_0^{(1)} = {}^1/_2$ for all our calculations) at the start of the first quench and $\phi_0^{(2)}$ is the volume fraction within one of the two phases at the start of the second quench. Table 1 shows the predicted positions of the fastest growing wavevector, based on $\phi_0^{(2)} = 0.33$, the composition on the coexistence curve for $\chi_1 = 0.0104$.

The predicted quench depth dependence of $\mathbf{k}_{max}$ is opposite to that seen in our simulations, suggesting that we are not able to capture the true early stages particularly for larger $\mathbf{k}$; however, the secondary growth factors do seem to be commensurate with the early stage growth laws at very low $\mathbf{k}$. We also note that the above calculations assume an infinite system, whereas the secondary phase separation is effectively occurring within restricted domains. The disparity between the early stage theory and our results for larger $\mathbf{k}$ is highlighted in Figure 9, where $R(\mathbf{k})/\mathbf{k}^2$ is plotted against $\mathbf{k}^2$. From eq 9 it is clear that such a plot should be linear.

The results shown thus far have been for quenches where χ_2 is identical to χ_f; hence, the scaling for each simulation is different. It is therefore difficult to make quantitative comparisons of the secondary structure between the three different secondary quenches, particularly with regards to the degree of secondary phase separation. Hence, we also conducted simulations in which the scaling ($\chi_f - \chi_s$) was fixed ($\chi_f = 0.0133$, $\chi_s = 0.01$), but χ_2, i.e., the secondary quench depth, was varied. The first quench depth ($\chi_1 = 0.0104$) was identical in each case. Clearly it is not to be expected that all quenches will result in a secondary structure; not only does the secondary quench depth have to be large enough that each domain becomes unstable, i.e.

$$\chi_2 \geq \frac{1}{2N\phi_0^{(2)}(1-\phi_0^{(2)})} \quad (11)$$

but also the favored secondary structure must be

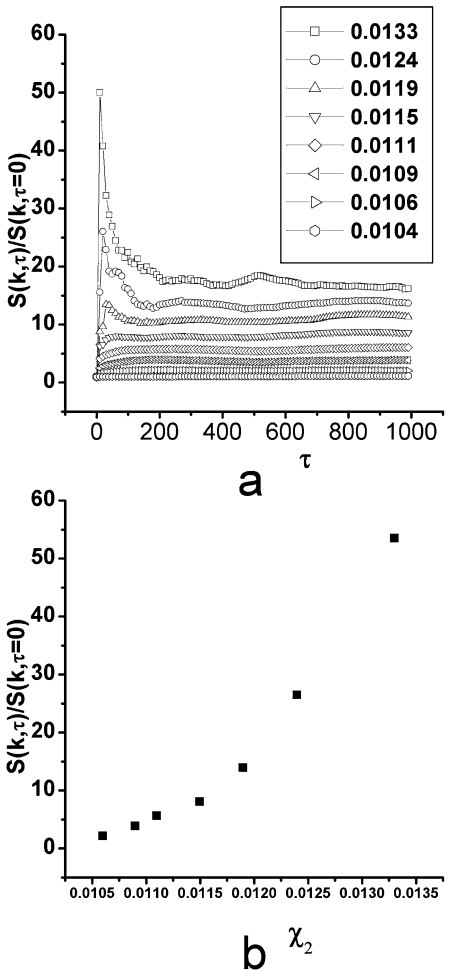

Figure 10. Plot showing (a) the change in the maximum value of the secondary structure factor with time for various values of χ_2 and (b) the peak value of the secondary structure factor for varying values of χ_2.

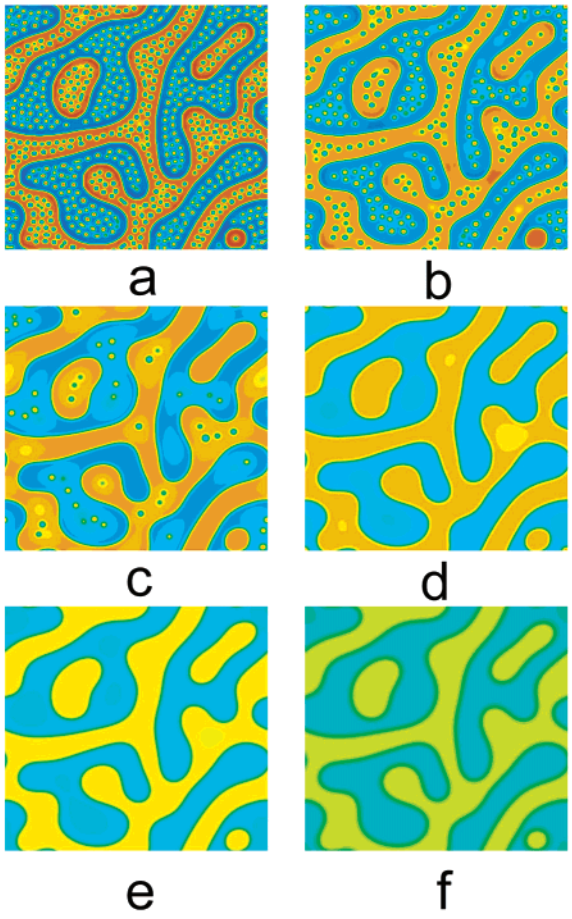

Figure 11. Secondary structure: (a) $\chi_2 = 0.0133$, $\tau_2 = 9$; (b) $\chi_2 = 0.0124$, $\tau_2 = 21$; (c) $\chi_2 = 0.0119$, $\tau_2 = 33$; (d) $\chi_2 = 0.0115$, $\tau_2 = 65$; (e) $\chi_2 = 0.0111$, $\tau_2 = 112$; and (f) $\chi_2 = 0.0106$, $\tau_2 = 166$ corresponding to the time of the maximum structure factor (Figure 10).

smaller than the length scale of the larger domain. This is illustrated in Figure 10, in which the maximum value of the structure factor with time for various secondary quench depths is shown. It can be seen that the deeper the quench, the greater the change of the structure factor with time. When the secondary quench depth is only slightly deeper than the primary quench, no secondary structure is observed, and only a slight growth in the structure factor is seen due to continued domain broadening. In Figure 11, the morphology at a time corresponding to the peak in the secondary structure factor is shown for various quench depths. Clearly, as would be expected, the greater the quench depth, the greater the degree of secondary phase separation and the finer the secondary morphology.

To quantify the secondary process further, we isolated domains in which $\phi > {}^1/_2$ at the start of the second quench and probed the dynamics by considering the time dependence of the variance defined by

$$\text{variance} = \frac{1}{N_T} \sum_{\substack{i,j \\ \phi_{i,j}(\tau_2=0) > 1/2}} [\phi_{i,j}(\tau_2) - \bar{\phi}(\tau_2)]^2 \quad (12)$$

The average $\bar{\phi}(\tau_2)$ was also only determined for lattice sites in which $\phi(\tau=0) > {}^1/_2$, and N_T corresponds to the number of such lattice sites. The advantage of eq 12, which can also be easily measured experimentally with

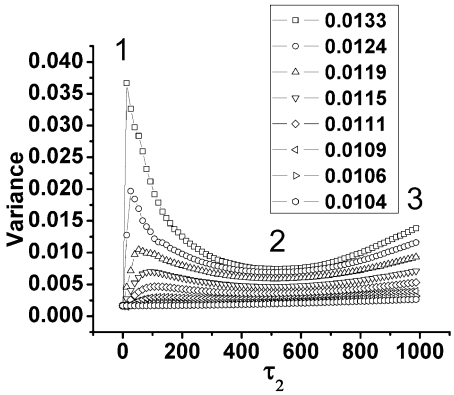

Figure 12. Variance of ϕ for various different second quench depths as indicated by the numbers in the inset. The numbers 1, 2, and 3 refer to the three stages of the second quench, as discussed in the text.

image analysis techniques, is that we remove factors due to the primary structure. In particular, when no secondary phase separation occurs, the variance only varies slightly from zero due to the random fluctuations.

As can be seen in Figure 12, as τ_2 increases, the variance goes through three distinct stages. At stage 1 the maximum degree of secondary phase separation occurs, and after this the secondary phase disappears; hence, the subsequent reduction in the variance. By stage 2, the secondary phase separation has been "absorbed" back into the larger phases, and the original

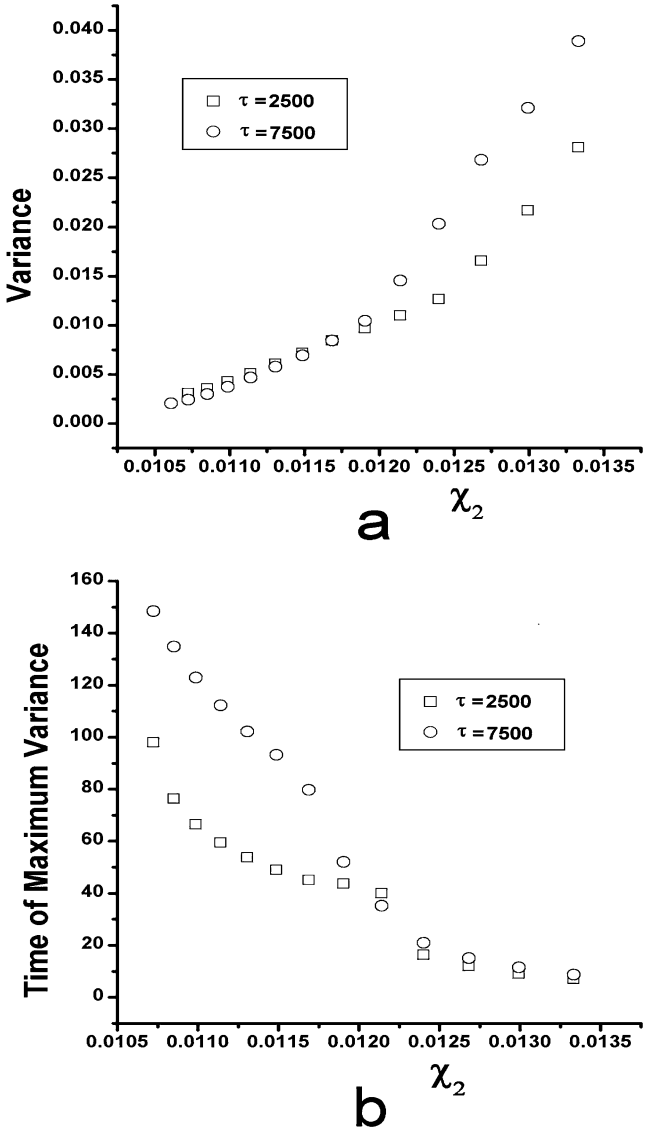

Figure 13. Comparison of (a) the maximum variance and (b) the time of the maximum variance with secondary quench depth χ_2 for a first quench of $\tau_1 = 2500$ and 7500.

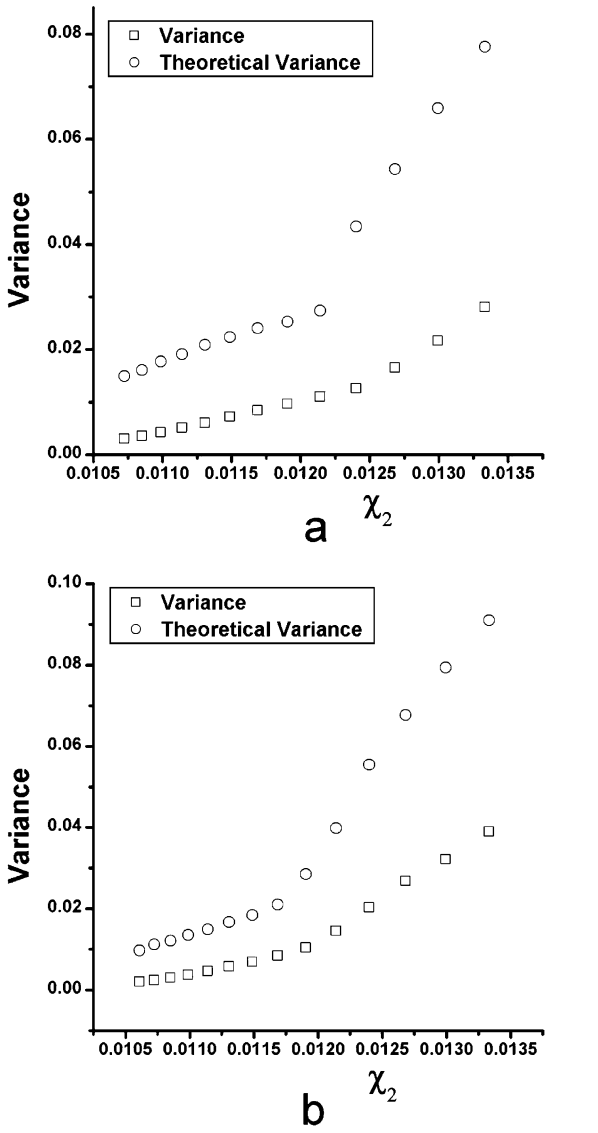

Figure 14. Comparison of the maximum theoretical variance and the maximum variance found by simulation for (a) first quench of $\tau_1 = 2500$ and (b) a first quench of $\tau_1 = 7500$.

morphology has been returned. Between stages 2 and 3 the domains continue to broaden so the variance again increases with τ_2 since the originally isolated regions with $\phi > {}^1/_2$ no longer correspond to the primary morphology. It can be seen that the deeper the quench the greater the changes in variance. When no secondary phase separation occurs, the variance still increases due to the domain broadening effects, but there is no peak.

The increased degree of secondary phase separation, as measured by the variance, is illustrated clearly in Figure 13a: as χ_2 increases, so does the maximum value of the variance. Similar trends can be seen for both $\tau_1 = 2500$ and $\tau_1 = 7500$, although the degree of secondary phase separation is greater for the latter case when $\chi_2 > 0.0120$. We also show in Figure 13b that the time at which the greatest secondary structure occurs decreases as the quench depth increases. It is interesting to note that there appears to be an abrupt change in behavior at $\chi_2 \approx 0.0120$ for $\tau_1 = 7500$ and $\chi_2 \approx 0.012\,25$ for $\tau_1 = 2500$, but the reasons for this are unclear.

The absolute value of the variance as illustrated in Figure 13 is clearly a useful tool for qualitative comparisons between quench depths; however, it is possible to further quantify the process since we can determine the maximum theoretical variance. We reasonably assume that the maximum degree of secondary phase separation corresponds to the two secondary phases attaining the coexistence compositions, ϕ' and ϕ'', associated with the secondary quench depth as determined by the binodal curve. First we need to determine the theoretical area that would be occupied by each of the two secondary phases using the Lever rule, $v'\phi' + v''\phi'' = v\bar{\phi}$ where the total area of the domain is v, and v' and v'' are the areas of the phases with compositions ϕ' and ϕ'', respectively. Since $v = v' + v''$, $v' = v[(\bar{\phi} - \phi'')/(\phi' - \phi'')]$ and $v'' = v[(\bar{\phi} - \phi)/(\phi'' - \phi')]$.

Hence, if we further assume sharp interfaces, the maximum theoretical variance corresponds to

$$\text{variance} = \frac{1}{v}[v'(\phi' - \bar{\phi})^2 + v''(\phi'' - \bar{\phi})^2] \qquad (13)$$

The minimum and maximum polymer concentrations (ϕ' and ϕ'') are determined from eq 3.

While the theoretical variance and the variance determined from the simulation follow the same trend, as shown in Figure 14, the secondary phase separation

is unable to reach "completion" before penalties due to interfacial energy become too costly, and diffusion enables larger scale rearrangement. It is also clear from Figure 14 that the larger the initial structure, the smaller the difference between the theoretical variance and the actual variance, in agreement with the observations of ref 22. This is due to the secondary phases being able to develop further before "interaction" with the primary structure becomes significant. Again there appears to be an abrupt change in behavior at $\chi_2 \approx 0.0120$ for $\tau_1 = 7500$ and $\chi_2 \approx 0.012\,25$ for $\tau_1 = 2500$.

Conclusions

We have explored the early stages of secondary phase separation following a two-step quench process, using a finite difference scheme for a spatially and temporally discretized version of the Cahn−Hilliard equation. The morphology development was probed by determining the structure factor. These results showed a secondary shoulder, associated with secondary phase separation, appearing immediately after the second quench, which shares features in common with the initial time dependence expected from the linearized Cahn−Hilliard theory. Differences arise due to the numerical difficulty of capturing the "true" early stages. In all cases the secondary structure reaches a maximum before the morphology relaxes back to the initial structure, but with a greater difference in composition between the two phases. As in experiments,[22−24] we find that the secondary structure is absorbed back into the primary structure while the primary structure coarsens. However, we do not observe coarsening of the secondary structures; this is probably due to the initial primary structure not having a significantly greater length scale than the secondary, although another possibility is the neglect of hydrodynamic effects. Achieving such a wide range of length scales with the resultant increase in time scales is beyond the scope of this study.

From the point of view of applications, we have quantified the degree of secondary phase separation as a function of time and quench depth by determining the variation of the variance within one of the primary domains. The time at which the maximum variance occurs corresponds to the optimally secondary phase separated structure. We have found that the secondary structure does not attain the theoretical maximum secondary structure, which would correspond to secondary domains possessing the equilibrium compositions expected from the coexistence curves. These predictions suggest further experiments that will enable theory to be quantifiably tested.

Acknowledgment. The authors acknowledge financial support from Cytec Engineered Materials.

References and Notes

(1) Cahn, J. W.; Hilliard, J. E. *J. Chem. Phys.* **1958**, *28*, 258.
(2) deGennes, P. G. *J. Chem. Phys.* **1980**, *72*, 4756.
(3) Pincus, P. *J. Chem. Phys.* **1981**, *75*, 1996.
(4) Binder, K. *J. Chem. Phys.* **1983**, *79*, 6387.
(5) Flory, P. J. *Principles of Polymer Chemistry*; Cornell University Press: Ithaca, NY, 1953.
(6) Rogers, T. M.; Elder, K. R.; Desai, R. C. *Phys. Rev. B* **1988**, *37*, 9638.
(7) Chakrabarti, A.; Toral, R.; Grunton, J. D.; Muthukumar, M. *J. Chem. Phys.* **1990**, *92*, 6899.
(8) Chakrabarti, A.; Toral, R.; Gunton, J. D.; Muthukumar, M. *Phys. Rev. Lett.* **1989**, *63*, 2072.
(9) Brown, G.; Chakrabarti, A. *J. Chem. Phys.* **1993**, *98*, 2451.
(10) Chakrabarti, A.; Gunton, J. D. *Phys. Rev. B* **1988**, *37*, 3798.
(11) Langer, J. S. *Acta Metall.* **1973**, *21*, 1649.
(12) Akcasu, A. Z.; Klein, R. *Macromolecules* **1993**, *26*, 1429.
(13) Huang, C.; Cruz, M. O. d. l. *Macromolecules* **1994**, *27*, 4231.
(14) Schichtel, T. E.; Binder, K. *Macromolecules* **1987**, *20*, 1671.
(15) Clarke, N. *Eur. Phys. J. E* **2001**, *4*, 327.
(16) Pagonabarraga, I.; Cates, M. E. *Macromolecules* **2003**, *36*, 934.
(17) Takenaka, M.; Hashimoto, T. *Phys. Rev. E* **1993**, *48*, 647.
(18) Balazs, A. C.; Ginzburg, V. V.; Qui, F.; Peng, G.; Jasnow, D. *J. Chem. Phys.* **2000**, *104*, 3411.
(19) Peng, G.; Qiu, F.; Ginzburg, V. V.; Jasnow, D.; Balazs, A. C. *Science* **2000**, *288*, 1802.
(20) Tanaka, H. *J. Phys.: Condens. Matter* **2000**, *12*, R207.
(21) Kwak, K. D.; Okada, M.; Chiba, T.; Nose, T. *Macromolecules* **1993**, *26*, 4047.
(22) Hayashi, M.; Jinnai, H.; Hashimoto, T. *J. Chem. Phys.* **2000**, *113*, 3414.
(23) Hashimoto, T.; Hayashi, M.; Jinnai, H. *J. Chem. Phys.* **2000**, *112*, 6886.
(24) Hayashi, M.; Jinnai, H.; Hashimoto, T. *J. Chem. Phys.* **2000**, *112*, 6897.
(25) Fialkowski, M.; Holyst, R. *J. Chem. Phys.* **2002**, *117*, 1886.
(26) Clarke, N. *Phys. Rev. Lett.* **2002**, *89*, 215506.
(27) Cahn, J. W. *J. Chem. Phys.* **1965**, *42*, 93.
(28) Cook, H. E. *Acta Metall.* **1970**, *18*, 297.
(29) Glotzer, S. C. *Annu. Rev. Comput. Phys.* **1995**, *2*, 1.
(30) de Gennes, P. G. *Scaling Concepts in Polymer Physics*; Cornell University Press: Ithaca, NY, 1993.

MA034718L